

Annual Review of Condensed Matter Physics
**Modeling Active Colloids:
From Active Brownian
Particles to Hydrodynamic
and Chemical Fields**

Andreas Zöttl¹ and Holger Stark²

¹Faculty of Physics, University of Vienna, Vienna, Austria; email: andreas.zoettl@univie.ac.at

²Institute for Theoretical Physics, TU Berlin, Berlin, Germany; email: holger.stark@tu-berlin.de

ANNUAL
REVIEWS **CONNECT**

www.annualreviews.org

- Download figures
- Navigate cited references
- Keyword search
- Explore related articles
- Share via email or social media

Annu. Rev. Condens. Matter Phys. 2023. 14:109–27

First published as a Review in Advance on
October 20, 2022

The *Annual Review of Condensed Matter Physics* is
online at conmatphys.annualreviews.org

<https://doi.org/10.1146/annurev-conmatphys-040821-115500>

Copyright © 2023 by the author(s). This work is licensed under a Creative Commons Attribution 4.0 International License, which permits unrestricted use, distribution, and reproduction in any medium, provided the original author and source are credited. See credit lines of images or other third-party material in this article for license information.



Keywords

microswimmers, numerical modeling, hydrodynamic and phoretic interactions, complex environments, active baths, active engines

Abstract

Active colloids are self-propelled particles moving in viscous fluids by consuming fuel from their surroundings. Here, we review the numerical and theoretical modeling of active colloids propelled by self-generated near-surface flows. We start with the generic model of an active Brownian particle taking into account potential forces and effective pairwise interaction, which include hydrodynamic and phoretic interactions. Also, the squirmer as a model microswimmer is introduced. We then discuss the explicit modeling of self-generated fluid flow and the full hydrodynamic-chemical coupling. Finally, we discuss recent advances in selected topics in which modeling of active colloids is used to study motion in crowded and complex environments, microrheology in active baths, active colloidal engines, adaptive responses of active colloids with the help of machine learning techniques, as well as effects of colloid and fluid inertia.

1. INTRODUCTION

Active colloids convert chemical or free energy and thereby perform autonomous directed motion. In contrast to externally driven particles, the direction of motion is set by an intrinsic orientation that can vary in time. Active colloids are a well-defined model system to investigate microscopic out-of-equilibrium phenomena such as emergent collective phenomena or the activity-induced phase behavior in a controllable way (1, 2). Furthermore, active colloids may have technological implications, for example, for cargo transport and (drug) delivery through microvessels, or they serve as building blocks for active, potentially self-assembling materials (3).

In principle, in light of condensed matter physics, we can see an active colloid from different angles, namely

- as an active agent operating out of equilibrium,
- as a (Brownian) microswimmer interacting through hydrodynamic, chemical, electric, or other fields,
- as a building block for active matter assembly, and
- as a machine that performs work running with “fuel” from its surrounding.

1.1. How Do Active Colloids Move?

When we think of active colloids, we have in mind a fixed shape, typically spherical, and the colloid can actively move without applying external forces in a fluid. Instead, it uses some sort of fuel from the surroundings to maintain, for example, a reaction on the colloidal surface, which eventually generates self-propulsion. In contrast, shape-deforming microswimmers or microorganisms swim forward by performing periodic nonreciprocal motion (4), whereas “dry” systems such as active granular matter operate and move out of equilibrium through vibrations of the carrying surface, as demonstrated, for example, in Reference 5.

How is it possible that colloids of fixed shape actively move in a homogeneous medium without applying forces? Most realizations of active colloids self-generate hydrodynamic flows \mathbf{u}_s at and tangential to their surfaces, as a result of fuel consumption. These self-generated phoretic flows close to the colloid surface can have different origins, but typically they are initiated by chemical reactions at the particle surface (6–8). The instantaneous orientation $\mathbf{e}(t)$ of the active colloid may be imprinted through the front–back asymmetry of Janus particles (8), through the presence of other phoretically active particles (9), or through spontaneous symmetry breaking as in active droplets (10).

There are various mechanisms for how self-propulsion based on the required near-surface flow fields \mathbf{u}_s evolves: Self-diffusiophoresis creates a tangential gradient ∇c of a chemical field $c(\mathbf{r}_s)$ at the surface location \mathbf{r}_s (7, 11), self-electrophoresis creates an electric potential gradient $\nabla \zeta$ (7), self-thermophoresis creates a temperature gradient ∇T (12–14), and binary fluid mixtures can locally demix so that a gradient in composition occurs (15). We do not aim here to describe the origins of the different phoretic flows; this is reviewed in detail elsewhere (6–8). We only point out that the surface flow is typically linear in the field gradient tangential to the surface,

$$\mathbf{u}_s(\mathbf{r}_s) = -\kappa(\mathbf{r}_s)\nabla\psi(\mathbf{r}_s), \quad 1.$$

where ψ can be any of the aforementioned or other phoretic fields and the prefactor κ depends on the specific coupling of the fields to the colloid surface. Here, we are interested in the consequences of the emerging hydrodynamic near-surface flows and the phoretic fields induced by the phoretic mechanisms. First and most importantly, the generated surface velocity field \mathbf{u}_s determines the

colloid's swimming speed and rotational velocity. For spherical colloids of diameter σ they are given by (6, 16)

$$\mathbf{v}_0 = v_0 \mathbf{e} = -\langle \mathbf{u}_s \rangle, \quad 2.$$

$$\boldsymbol{\omega}_0 = \frac{3}{\sigma} \langle \mathbf{u}_s \times \mathbf{n} \rangle, \quad 3.$$

where $\langle \dots \rangle$ indicates a surface average and \mathbf{n} the local surface normal. Often the surface velocity field \mathbf{u}_s is axisymmetric as, for example, in half-coated self-propelled Janus colloids, and hence the intrinsic angular velocity $\boldsymbol{\omega}_0$ vanishes. However, both the position and the orientation of the active colloid are influenced by random noise. This results in a persistent random walk, which renders its trajectory diffusive in times greater than the persistence time, indicating the time during which the active colloid follows a straight path (1). We quantify it in Section 2.1.

A standard approach is to abstract from the concrete mechanism, which generates self-propulsion. Then the active colloids are considered as active Brownian particles (ABPs) with swimming (\mathbf{v}_0) and rotational ($\boldsymbol{\omega}_0$) velocities that interact by hydrodynamic and phoretic flow, which they generate themselves, and also by potential forces such as hard-core interactions.

1.2. Interacting Active Colloids

The specific hydrodynamic and phoretic fields, as well as the particle shape, become important when considering interacting active colloids or colloids interacting with either confining surfaces or complex environments. In these situations the specific forms of the self-generated fields play a crucial role in the dynamic behavior. When two or more active colloids are sufficiently close, they interact with each other through the hydrodynamic and phoretic fields they create and also through short-range repulsive or attractive interactions. This modifies their swimming velocities and, even more importantly, rotates active colloids so that they change their swimming directions.

The self-generated flow fields of active colloids are governed by the Stokes equations, which describe the hydrodynamics of viscous fluids at the micron scale, where the Reynolds number typically is very small; hence, inertia is negligible (1). The Stokes equations are linear second-order differential equations for the fluid flow $\mathbf{u}(\mathbf{r}, t)$ and pressure field $p(\mathbf{r}, t)$,

$$\eta \nabla^2 \mathbf{u} = \nabla p \quad \text{and} \quad \nabla \cdot \mathbf{u} = 0, \quad 4.$$

where η is the shear viscosity of the fluid, and the second part in Equation 4 is due to fluid incompressibility. In a bulk fluid the flow fields of active colloids are uniquely determined by the specific form of the self-generated surface velocity field \mathbf{u}_s , but they are distorted in the presence of objects such as other colloids or bounding surfaces. The solution of the Stokes equations can be expanded into hydrodynamic multipoles similar to the multipole expansion in electrostatics. The leading-order solution is the stokeslet flow field \mathbf{u}_{St} , which belongs to a particle dragged by an external force through the fluid. However, self-propelling active colloids are force-free by definition and, therefore, do not create a stokeslet flow field if external forces are not applied. Instead, their intrinsic flow fields have to be described by higher-order singularities (1, 17), and the most important ones for active colloids are force dipoles \mathbf{u}_{FD} and source dipoles \mathbf{u}_{SD} . While the force-dipole field consists of two nearby stokeslets with opposing forces, the source-dipole field is composed of two infinitesimally close source and sink fields, which each can be described as $\propto \nabla \frac{1}{r}$. Thus, they are potential flows and in combination fully equivalent to an electric dipole field. The specific contributions of the flow-field multipoles can analytically be calculated for spherical active colloids and depend on the surface velocity field \mathbf{u}_s of the active colloid oriented along the unit

vector \mathbf{e} . In general, for any shape of the active colloid, the leading-order flow fields are given by

$$\mathbf{u}_{\text{St}}(\mathbf{r}) = \frac{f}{8\pi\eta r} [\mathbf{e} + (\hat{\mathbf{r}} \cdot \mathbf{e})\hat{\mathbf{r}}], \quad 5.$$

$$\mathbf{u}_{\text{FD}}(\mathbf{r}) = \frac{p}{8\pi\eta r^2} [-1 + 3(\mathbf{e} \cdot \hat{\mathbf{r}})^2] \hat{\mathbf{r}}, \quad 6.$$

$$\mathbf{u}_{\text{SD}}(\mathbf{r}) = \frac{q}{8\pi\eta r^3} [-\mathbf{e} + 3(\mathbf{e} \cdot \hat{\mathbf{r}})\hat{\mathbf{r}}], \quad 7.$$

where we included the stokeslet term with point force f for completeness, p and q are the respective strengths of the force dipole and source dipole, and $\hat{\mathbf{r}}$ is the radial unit vector. When $p > 0$, the force-dipole flow field is extensile, and the active colloid behaves as a pusher, whereas for $p < 0$ it is contractile with the active colloid being a puller. This notation is motivated by swimming strokes and corresponding flow fields of swimming microorganisms (4). Indeed, experimental measurements of flow fields of active colloids demonstrated how the leading-order flow field is related to the surface velocity \mathbf{u}_s induced by catalytic activity (18).

In the far-field limit (separation much larger than particle radius), the leading-order multipole fields determine how hydrodynamically interacting particles are reoriented. However, when particles are close to each other, potentially strong near fields, for example, generated by the tangential surface velocity fields, determine their reorientation (19, 20). The near fields do not have generic forms as multipole fields but are specific for each problem. Hydrodynamic and phoretic fields crucially determine the collective dynamics of active colloids. Here, theoretical modeling and computer simulations are useful because they allow us to access these fields together with the colloidal dynamics. In contrast, measuring hydrodynamic and phoretic fields in experiments, and also how they vary in time, is very challenging.

Similarly, the phoretic fields are governed by linear second-order differential equations such as the diffusion equation for the chemical field, the heat equation for temperature fields, or Poisson's equation for the electric potential. Often, a quasistatic limit is used so that the diffusion equation also becomes a Poisson equation. Nevertheless, the fields $\psi(\mathbf{r}, t)$ are time-dependent because they move with the colloids located at positions $\mathbf{r}_i(t)$. Sufficiently far from the colloid, the monopole term of a point source dominates and the quasistatic field becomes (21, 22)

$$\psi(\mathbf{r}, t) \sim \sum_i \frac{1}{|\mathbf{r} - \mathbf{r}_i(t)|}, \quad 8.$$

with constant prefactors that depend on the specific phoretic mechanisms. Although the phoretic fields decay with r^{-1} in leading order, their gradients $\nabla\psi$, which determine the interactions between colloids as we outline in Section 2.2.2, decay as r^{-2} .

1.3. Outline

In this review, we focus on modeling active matter on the particle level and not on field-based continuum modeling, which is reviewed, for example, in Reference 23. In Section 2, we introduce the modeling of active colloids at different levels of complexity. We start with the simplest level of an ABP, where potential forces are included, and then introduce different types of effective pairwise interactions. They include attractive forces and, in particular, phoretic and hydrodynamic interactions. To prepare the following discussion, we also introduce the squirmer as a model microswimmer. In Section 3, we turn to a discussion of more accurately modeling the hydrodynamic and phoretic fields as well as approaches, where they are explicitly coupled to each

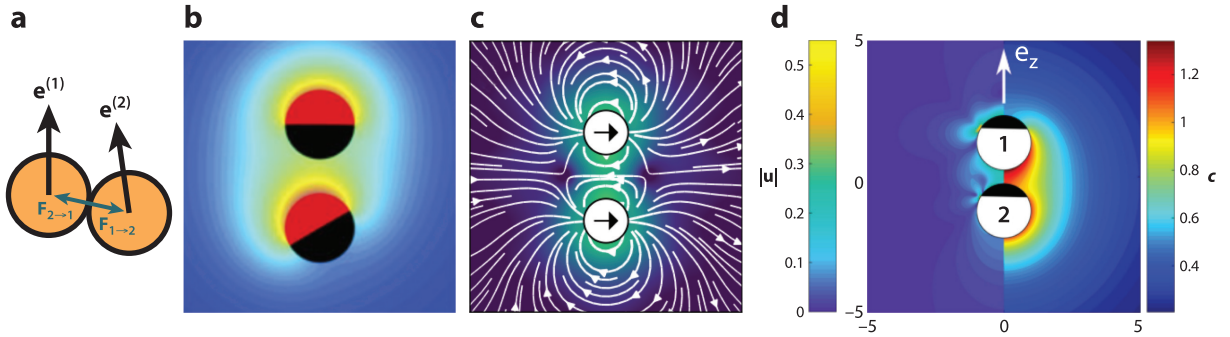


Figure 1

Different levels of modeling interacting active colloids. (a) Purely repulsive ABPs with intrinsic orientations $\mathbf{e}^{(i)}$ interacting through mutual short-range repulsive interactions $\mathbf{F}_{2 \rightarrow 1} = -\mathbf{F}_{1 \rightarrow 2} = -\nabla^{(1)}U$. (b) Phoretic interactions between catalytically active colloids. (c) Hydrodynamic interactions between two squirmers moving in a monolayer. (d) Hydrodynamic-chemical coupling between active colloids. Left: Magnitude of hydrodynamic flow field. Right: Chemical field. Panel *b* adapted with permission from Reference 24. Panel *c* provided by A. Zantop. Panel *d* adapted with permission from Reference 25; copyright 2019 American Physical Society.

other. In Section 4, we present a personal selection of recent developments in the field, where particle-based modeling is also applied. We finish with a short conclusion.

2. MODELING ACTIVE COLLOIDS AS ACTIVE BROWNIAN PARTICLES

2.1. Purely Repulsive Active Brownian Particles

The simplest model for describing the behavior of active colloids is the ABP model, which is heavily used when studying interacting active colloids (1, 2). In the generic, most simple ABP model, hydrodynamic, phoretic, and essentially all other interactions between active colloids are neglected, except steric repulsion. It assumes that they move with an intrinsic speed v_0 along a polar orientation, $\mathbf{e}(t)$, under the influence of translational and rotational random noise. Furthermore, taking into account a volume-exclusion interaction potential U , the overdamped Langevin equations for the i th ABP become (see **Figure 1a**),

$$\frac{d}{dt}\mathbf{r}^{(i)} = v_0\mathbf{e}^{(i)} - \frac{D}{k_B T}\nabla^{(i)}U + \sqrt{2D}\boldsymbol{\xi}^{(i)}, \quad 9.$$

$$\frac{d}{dt}\mathbf{e}^{(i)} = \sqrt{2D_r}\boldsymbol{\xi}_r^{(i)} \times \mathbf{e}^{(i)}, \quad 10.$$

where the components of the random variables $\boldsymbol{\xi}^{(i)}$ and $\boldsymbol{\xi}_r^{(i)}$ are usually modeled as Gaussian random white noise with zero mean and unit variance, $\langle \xi_j^{(i)}(t)\xi_k^{(i')}(t') \rangle = \delta_{jk}\delta^{ii'}\delta(t-t')$, and the same applies to $\boldsymbol{\xi}_r^{(i)}$. The strengths of the translational and rotational noise are determined by the translational and rotational diffusion constants D and D_r , respectively. The solution of Equations 9 and 10 for a single ABP or noninteracting ABPs ($U = 0$) is a persistent random walk, where the persistence length of the trajectories is given by v_0/D_r (1, 2). Here, D_r^{-1} is the time on which the orientational correlations of $\mathbf{e}(t)$ decay exponentially, which we mentioned as persistence time in Section 1.1. It is also the time that an active particle swimming against a wall needs to orient away from the wall by rotational diffusion so that it can leave the wall. The relative strength of active to random motion is quantified by the Péclet number, $\text{Pe} = v_0\sigma/D$, the ratio of times the active particle needs to either move by activity or to diffuse a particle diameter σ , respectively. The alternative rotational

Péclet number, $\text{Pe}_r = v_0/(D_r\sigma)$, is the ratio of persistence length to particle diameter σ and a clear measure for the persistence of swimming against the action of rotational noise. Thereby, it crucially determines the dynamics of active colloids.

The potential U ensures that particles do not overlap substantially. It is realized by pairwise potentials U_{ij} such that $U = \sum_{i < j} U_{ij}(r_{ij})$ with $r_{ij} = |\mathbf{r}^{(i)} - \mathbf{r}^{(j)}|$. Typically, for spherical colloids this is included by means of a purely repulsive short-range potential, often of the Weeks–Chandler–Andersen (WCA) type,

$$U_{ij}^{\text{WCA}}(r) = \begin{cases} 4\epsilon \left[\left(\frac{\sigma}{r}\right)^{12} - \left(\frac{\sigma}{r}\right)^6 + \frac{1}{4} \right], & \text{if } r < 2^{1/6}\sigma \\ 0, & \text{otherwise} \end{cases}, \quad 11.$$

with ϵ being the strength of the potential, where $\epsilon \sim k_B T$ models soft- and $\epsilon \gg k_B T$ hard-sphere interactions. When pure Brownian noise at temperature T is considered, the relation $D_r = 3D/\sigma^2$ is valid, which follows from the Einstein relations $D = k_B T/\gamma$ and $D_r = k_B T/\gamma_r$ (with $\gamma = 3\pi\eta\sigma$ and $\gamma_r = \pi\eta\sigma^3$ the translational and rotational friction coefficients, respectively). Equations 9–11 are then solved using Brownian dynamics (BD) simulations (1).

In both two dimensions (2D) and three dimensions (3D), the system phase-separates into a dense and gas-like phase at sufficiently large particle density ρ and rotational Péclet number Pe_r (26–28). Thus, collisions between active colloids are sufficiently frequent so that the mean collision time is smaller than the time D_r^{-1} a colloid needs to reorient and leave a cluster. This motility-induced phase separation (MIPS) has extensively been investigated as a prototypical and generic feature of a nonequilibrium, active matter system (see, e.g., the review in Reference 29). One might think that the simple ABP model, which completely neglects any hydrodynamic and phoretic interactions, does not describe any real system. However, this is not the case. For example, in the system of collectively moving active Janus colloids, which self-propel by heating them with laser light that locally demixes a binary fluid, thermal reorientation dynamics is considered to be dominant over hydrodynamic, phoretic, and other attractive interactions (27). Here, when rotational noise is sufficiently small and particle density sufficiently large, particles become trapped when pushing against each other, which allows more and more particles to join and form a cluster. Hence, the simple ABP model is the prototypical model for studying the resulting MIPS (26–30) or more general mechanisms of active self-assembly (3). Furthermore, dense clusters of ABPs display various dynamic and structural features that are known from dense colloidal systems in equilibrium, such as jamming, crystallization, and hexatic phases (26, 28, 30). Motivated by experiments mainly conducted in a monolayer of active colloids, most of the ABP simulations have been performed in 2D (26, 27, 30) or in a quasi-2D geometry (31). However, the main features of the observed phase behavior in 2D still hold in 3D (32, 33).

Besides the canonical spherical shape (or disk shape in 2D), several types of nonspherical ABPs have been investigated, most prominently active Brownian dumbbells (34) and rods (35–37), for example, by spheres rigidly connecting to each other. The main difference of these elongated active particles compared to spherical particles is an extra nematic aligning mechanism for interacting rods due to the interplay of self-propulsion and steric interactions (37).

Furthermore, the classical ABP model with intrinsic velocity has been extended to also include an intrinsic angular velocity, which was then termed “circle swimmer” (38). This model is motivated by chiral biological microswimmers such as bacteria moving in circles close to surfaces, but also asymmetric phoretically active colloids have been designed (39). Other models only consider an intrinsic angular velocity without translational self-propulsion, also termed spinners (40). However, for active spinners with spherical shape the ABP model is not sufficient because hydrodynamic interactions play an essential role (41, 42).

All in all, the simplest ABP model with pure repulsion has been heavily used. It contains a minimum number of ingredients—self-propulsion, random reorientation, and hard-core interaction—characteristic for active colloids. As such, it is used to describe and quantify principal features of active matter, which we also address in Section 4. However, in real active colloidal systems particle interactions are more complex, which needs modifications in the modeling approach, as discussed in the following.

2.2. Active Brownian Particles with Effective Pairwise Interactions

In addition to the purely repulsive potential, we now consider other forms of interactions, which are specific for certain situations. They include attractive, phoretic, and hydrodynamic interactions, which we treat on the pairwise level. We also introduce the squirmer as a model microswimmer.

2.2.1. Attractive interactions. Similar to those of passive colloidal systems, the interaction and collective behavior of active colloids can be significantly influenced by short-range attractive interactions (43, 44). In combination with repulsive interactions due to volume exclusion, a canonical form to describe and model such attractive forces is the Lennard–Jones (LJ) potential, which is described by the first line of the WCA potential shown in Equation 11 but with the cutoff distance r_c removed or shifted to a larger value such that the attractive part is included.

As a result of activity and short-range attraction, active colloids show a re-entrant phase behavior in 2D depending on particle activity (26) as well as dynamic cluster formation in 2D and 3D (45, 46). All in all, adding attractive interactions allows one to explain cluster formation observed in experiments at relatively low densities (43, 44).

2.2.2. Phoretic interactions. As outlined in the introduction, various self-phoretic mechanisms rely on the emergence of phoretic fields centered around the particles, which reorient with the intrinsic particle direction, \mathbf{e} . Now, when a phoretic particle moves in the vicinity of other particles, it interacts with the phoretic field $\psi(\mathbf{r}, t)$ created by all the other particles (or by an external source). This modifies its translational and angular velocities, which we therefore term a field-mediated phoretic interaction between active colloids. We quantify them by field-dependent velocities \mathbf{v}_ψ and angular velocities $\boldsymbol{\omega}_\psi$ (47, 48), which in the simplest form (assuming the intrinsic velocity v_0 not influenced by the field) modify the equation of motion of the active colloids to

$$\frac{d}{dt} \mathbf{r}^{(i)} = v_0 \mathbf{e}^{(i)} + \mathbf{v}_\psi^{(i)} - \frac{D}{k_B T} \nabla^{(i)} U + \sqrt{2D} \boldsymbol{\xi}^{(i)}, \quad 12.$$

$$\frac{d}{dt} \mathbf{e}^{(i)} = \left(\boldsymbol{\omega}_\psi^{(i)} + \sqrt{2D_r} \boldsymbol{\xi}_r^{(i)} \right) \times \mathbf{e}^{(i)}, \quad 13.$$

where $\mathbf{v}_\psi^{(i)}$ and $\boldsymbol{\omega}_\psi^{(i)}$ are proportional to the gradient of the phoretic field at position $\mathbf{r}^{(i)}$, $\nabla \psi(\mathbf{r}^{(i)}, t)$, and they also depend on the specific surface properties of the active colloids (21, 22).

The solutions of Equations 12 and 13 (or modifications of them) lead to a diverse dynamic behavior, ranging from dynamic clustering (47) to aster formation (48) and collective oscillations (22, 48), also in mixtures with passive colloids (49). In addition, these equations were used to describe phototaxis of synthetic microswimmers (15).

2.2.3. Hydrodynamic interactions. Active colloids interact with each other through their self-generated hydrodynamic flow fields. When they are sufficiently distant from each other (far-field approximation), the instantaneous hydrodynamic flow field created by all colloids can be approximated simply by the sum of flow fields $\mathbf{u}^{(i)}(\mathbf{r}; \mathbf{r}^{(i)}(t), \mathbf{e}^{(i)}(t))$, each created by colloid i

located at $\mathbf{r}^{(i)}(t)$ and oriented along $\mathbf{e}^{(i)}(t)$. We write it as $\mathbf{u}^{(i)}(\mathbf{r}, t)$ for short. Now, each of these individual field contributions may be decomposed into hydrodynamic multipoles, with force dipoles (Equation 6) in leading order or a stokeslet (Equation 5) if external forces such as gravity act. The dynamics of the hydrodynamically interacting active colloids can be treated by the same Equations 12 and 13, but instead of the phoretic velocities the colloids now experience flow-field-induced velocities $\mathbf{v}_{\text{HI}}^{(i)}$ and angular velocities $\boldsymbol{\omega}_{\text{HI}}^{(i)}$. For far-field hydrodynamic interactions between spherical colloids, they are governed by Faxén's laws applied to the flow fields initiated by all other active colloids ($j \neq i$),

$$\mathbf{v}_{\text{HI}}^{(i)}(t) = \sum_{j \neq i} \left[1 + \frac{\sigma^2}{24} (\nabla^{(i)} \cdot \nabla^{(j)}) \right] \mathbf{u}^{(j)}(\mathbf{r}, t), \quad 14.$$

$$\boldsymbol{\omega}_{\text{HI}}^{(i)}(t) = \frac{1}{2} \sum_{j \neq i} \nabla^{(i)} \times \mathbf{u}^{(j)}(\mathbf{r}, t). \quad 15.$$

The second term on the right-hand side of Equation 14 takes into account that the active particles have a finite extent. Often it can be neglected. Such far-field interactions can be used to model dilute suspensions of active colloids where colloid–colloid collisions and, hence, near-field effects are negligible. For example, it has been used to model fluid pumps generated by active colloids in a harmonic potential (50). Even when thermal noise is negligible, these hydrodynamic far-field interactions cause random reorientations in interacting active colloidal suspensions and thereby contribute to the effective rotational diffusion of interacting colloids. However, in dilute and particularly semidilute suspensions, occasional close encounters of active colloids greatly enhance this effective hydrodynamic rotational diffusion. This can only be understood by hydrodynamic near fields, whereas far-field interactions alone substantially underestimate diffusion in three-dimensional active colloidal suspensions (51, 52).

Hence, in order to obtain a meaningful description of hydrodynamically interacting active colloids in the semidilute or dense regime, it is important to include hydrodynamic near-field interactions (20, 52, 53). An attempt to correctly include them together with far-field hydrodynamic interactions in the equations of motion of active colloids, with prescribed surface flow fields $\mathbf{u}_s^{(i)}$, is presented in Reference 20. The key is to correctly calculate the generally strong near-field interactions and to find a reasonable interpolation between far- and near-field contributions (19, 20). However, in order to fully capture the hydrodynamic field on all distances, it has to be determined explicitly, as described in Section 3.1.

2.2.4. The squirmer model microswimmer. A canonical model for studying hydrodynamic interactions of spherical (but also elongated) active colloids is the squirmer, originally introduced to model swimming microorganisms (54, 55). The squirmer swims with the help of an imprinted, stationary and axisymmetric velocity field \mathbf{u}_s at its surface. Typically, \mathbf{u}_s is taken tangential to the surface of the spherical active colloid along the polar direction, $\mathbf{u}_s = u_\theta(\theta)\hat{\boldsymbol{\theta}}$. Then, it is expanded into surface velocity modes B_n using Legendre polynomials $P_n(\cos \theta)$, where $\cos \theta = \mathbf{e} \cdot \hat{\mathbf{r}}_s$ with the unit vector $\hat{\mathbf{r}}_s$ pointing from the colloid center to its surface (55),

$$u_\theta(\theta) = \sum_{n=1}^{\infty} B_n \frac{2}{n(n+1)} \sin \theta \frac{dP_n(\cos \theta)}{d \cos \theta} = B_1 \sin \theta + B_2 \sin \theta \cos \theta + \dots \quad 16.$$

The swimming speed of the squirmer is calculated using Equation 2, and one finds $v_0 = 2B_1/3$; thus, it is solely determined by B_1 (55), whereas all surface modes B_n contribute to the flow field around the squirmer. The leading-order flow field is the hydrodynamic force-dipole field (Equation 6), which emerges from mode B_2 with force-dipole strength $p = -\pi \sigma^3 \eta B_2/2$, where $B_2 < 0$ models pushers and $B_2 > 0$ models pullers. When $B_2 = 0$, the leading-order flow field decays as

r^{-3} . It belongs to either a source-dipole field (Equation 7) generated by surface mode B_1 or a force-quadrupole field through B_3 . Often, a minimal squirmer model is employed, which only considers modes B_1 and B_2 . In contrast, phoretically active Janus colloids with half or partial coating can have more complicated surface velocity fields that require a larger number of surface modes (13, 18). They are, in particular, significant when near-field hydrodynamic interactions of these active colloids need to be considered. Finally, nonaxisymmetric surface fields generate additional flow field contributions and active rotation of colloids (56, 57).

3. EXPLICIT MODELING OF HYDRODYNAMIC AND CHEMICAL FIELDS

Using effective interactions between active colloids, as discussed in Section 2.2, allows efficient simulation of a large number of interacting colloids. However, this approach does not fulfill the correct boundary conditions of the hydrodynamic and phoretic fields at the colloids' surfaces, which is crucial, in particular, for dense suspensions, where near fields become relevant and there is screening by the presence of the other colloids. Therefore, an explicit modeling of hydrodynamic and chemical fields using the governing field equations is necessary. Methods to explicitly solve these field equations, namely the (Navier-)Stokes equations and the reaction-diffusion equation for self-diffusiophoretic colloids, are discussed below.

3.1. Explicit Modeling of Self-Generated Fluid Flow

In order to determine the full hydrodynamic flow field that fulfills the correct boundary condition at the surface of colloid i , $\mathbf{u}(\mathbf{r}, t)|_{\mathbf{r}=\mathbf{r}_s^{(i)}} = \mathbf{u}_s^{(i)}(\mathbf{r}_s^{(i)}(t), \mathbf{e}^{(i)}(t))$, explicit numerical simulations are necessary, as described below. We focus here on modeling hydrodynamic interactions between active colloids—the coupled hydrodynamic-phoretic modeling is described in Section 3.2. Due to its simple yet generic implementation of microswimmers propelled by surface flow, many studies use the squirmer model.

3.1.1. Non-Brownian active colloids in (Navier-)Stokes flow. Due to the micron size of active colloids, the Reynolds number is very small and fluid dynamics can be approximated in many situations by the Stokes equations (Equation 4). The first explicit numerical simulation of two interacting squirmers in Stokes flow has been performed in Reference 19 based on the boundary element method (BEM). It solves an integral equation equivalent to the Stokes equations using surface triangulations of interacting spherical (19) or ellipsoidal (51) squirmers. To simulate the collective motion of many squirmers at a specific volume fraction, one needs a simulation domain of finite extent, which is often realized by periodic boundary conditions. When using the Stokesian dynamics (SD) method, the Ewald summation technique is needed to correctly account for the long-range hydrodynamic interactions in combination with the periodic boundary conditions (51). In order to correctly simulate near-field hydrodynamics in concentrated suspensions, lubrication corrections have to be included. Then, it has been demonstrated that concentrated suspensions of squirmers in 3D develop polar order due to hydrodynamic interactions (58) and form clusters when moving in a monolayer (51). Another approach for simulating a large number of squirmers is the force coupling method (FCM), where the emerging polar order has also been analyzed for nonsteady and ellipsoidal squirmers (59). Finally, a method reminiscent of SD solves the Stokes equations around collectively squirming disks in 2D, which shows that in this system hydrodynamic interactions suppress cluster formation in the absence of attractive interactions (60). Altogether, all these methods rely on the linearity of the Stokes equations.

In order to simulate effects of a nonzero Reynolds number, one option is a direct numerical solution of the full Navier–Stokes equations. This has, for example, been achieved using a Lagrange-multiplier-based finite volume method to show inertial effects on pairwise squirmer–squirmers interactions (61).

3.1.2. Coarse-graining methods for Navier–Stokes flow. Alternative approaches to simulate the hydrodynamics around active colloids are coarse-graining methods such as multiparticle collision dynamics (MPCD; reviewed in Reference 62) or the lattice Boltzmann (LB) method (see, for example, References 63 and 64). They allow modeling of a large number of interacting colloids and the inclusion of complex boundaries. While the LB method evolves the distribution function for the flow velocity field based on the Boltzmann transport equation, MPCD simulates point-like effective fluid particles and therefore includes thermal noise intrinsically.

The squirmer model was first implemented using MPCD in Reference 65 for a single swimmer, then for two interacting squirmers (66), and then for a squirmer in wall-bounded flow (67). Also, a version of MPCD with decreased compressibility has been developed (68). The collective motion and clustering of hydrodynamically interacting squirmers have extensively been studied in a monolayer (31, 52, 69–71), where also a Wigner fluid and swarming were identified (70). In 3D and under gravity, squirmers exhibit very dynamic sedimentation profiles (72), and when adding bottom-heaviness, additional states like plumes, convective rolls, and spawning clusters occur (73), driven by gyrotactic cluster formation. Because MPCD includes thermal noise, it allows us to simulate squirmers at finite Péclet numbers in the presence of the thermally fluctuating hydrodynamic flow field. The specific surface velocity modes of squirmers at finite Péclet number strongly influence their collective behavior in a monolayer (31, 52, 69). The occurrence of MIPS is often suppressed compared to simple ABPs, but that also depends on the specific settings such as dynamics in 2D or quasi-2D, bounding walls and wall-hydrodynamic interactions, squirmer reorientation only in 2D or in 3D, zero or finite Reynolds number, and fluid (in-)compressibility (20, 31, 52, 60, 69). Furthermore, elongated squirmer rods (74) and squirmer ellipsoids (69) in a monolayer show clustering, polar order, and active turbulence (71, 75).

The LB method was first applied to two-dimensional active colloids and was eventually extended to hydrodynamically interacting squirmers in 3D (63). A very accurate implementation of a squirmer and its flow fields in LB has been proposed in Reference 64. The collective dynamics of many squirmers in a bulk fluid in 3D (76) and in the presence of attractive interactions (46) demonstrates the importance of hydrodynamic flow fields in active colloidal suspensions.

3.2. Explicit Modeling of Hydrodynamic-Chemical Coupling

Self-phoresis in anisotropic active colloids, such as Janus colloids catalyzing reactions at their surfaces, generates anisotropic phoretic fields. Their gradients induce tangential surface flows \mathbf{u}_s , as demonstrated in Equation 1, which uniquely define the flow fields around active colloids using the Stokes equations (Equation 4). In turn, the flow field \mathbf{u} determines the spatiotemporal evolution of the phoretic field $\psi(\mathbf{r}, t)$, for example, of a chemical field $c(\mathbf{r}, t)$ that evolves according to an advection-diffusion equation,

$$\frac{\partial c}{\partial t} + \mathbf{u} \cdot \nabla c = D_c \nabla^2 c, \quad 17.$$

where D_c is the diffusion constant of the chemical substance. This equation is supplemented by a boundary condition at the colloid surface, where the chemical is produced. Typically, the diffusion of the chemical is fast and the time-derivative in Equation 17 can be neglected such that a quasistatic field evolves.

The coupled equations for fluid flow (Equation 4) and phoretic field (Equation 17) have to be solved self-consistently using the appropriate boundary conditions for both fields at the surfaces of the colloids. A single colloid in bulk then carries with it a flow and phoretic field while moving, which are static in the comoving frame of the colloid. Thus, also the surface flow field is static as in a squirmer. Now, if these colloids interact with each other or a bounding surface, their phoretic fields ψ and the resulting surface velocities \mathbf{u}_s depend on the surrounding colloids or the distance to the bounding surface and, therefore, they change continuously. So, assuming a prescribed static surface velocity field as in a squirmer strictly is not valid anymore (77). A special case arises for self-phoretic isotropic colloids: A single colloid creates an isotropic chemical field around itself but not a flow field. Therefore, it does not move for sufficiently small solute Péclet number $\text{Pe}_c = v_a \sigma / D_c$, i.e., for fast chemical diffusion D_c or for low surface activity of the colloid, which is quantified by the associated characteristic velocity v_a (10). However, in the presence of other colloids their isotropic symmetry is broken, leading to fluid flow and self-propulsion (9, 78). Alternatively, the isotropic symmetry of a single self-phoretic colloid is broken beyond a critical solute Péclet number and the colloid moves (10). This is similar to active droplets that start to swim when spontaneous symmetry breaking generates Marangoni flow close to the droplet surface (79).

Different methods have been used in recent years to accurately model the dynamic evolution of flow fields and chemical fields of interacting catalytically active colloids or of active colloids interacting with bounding surfaces. Approaches to determine the chemical field using BEM (80) and semianalytic methods (81) have been coupled to the hydrodynamic problem using the reciprocal theorem. They investigate the hydrodynamic-chemical coupling of a single active colloid interacting with a bounding wall and identify different dynamic regimes depending on surface activity. For two interacting colloids analytic solutions of chemical and hydrodynamic fields for specific configurations have been derived using bispherical coordinates (24, 82, 83). Based on phoretic-field expressions, semianalytic solutions for the flow field of more general configurations can be calculated through the method of reflections (24, 25), which include far-field expressions only valid in the dilute regime as used in References 84 and 85. Studying the collective motion of many interacting chemically active colloids requires numerical methods that couple hydrodynamic to chemical fields. Indeed, recently several methods have been successfully applied for investigating collective phenomena in such systems. First, reactive multiparticle collision dynamics (R-MPCD) enables explicit simulation of different chemical species and their reactions together with hydrodynamic flow fields including thermal motion (86, 87). MPCD has also been coupled to temperature gradients in collectively moving self-thermophoretic colloids (88). Second, large-scale LB simulations are used to solve for the flow fields of self-diffusiophoretic particles and, in combination with the finite-difference method, to determine the chemical field from the advection-diffusion equation, where hydrodynamic-chemical effects lead to arrested cluster formation (89). Another approach employs the BEM (25) or the FCM together with a multipole expansion of the chemical field (90). In summary, in contrast to methods relying on far-field solutions (84, 85), explicit modeling of hydrodynamic-chemical fields allows us to account for correct near-field effects, which are important when active colloids come close to each other. However, the role of the interplay of hydrodynamic and phoretic fields in dense active colloidal suspensions is complex and depends on the specific model assumptions. We expect this to be subject to further investigations in the near future.

4. SELECTED TOPICAL APPLICATIONS OF MODELING ACTIVE COLLOIDS

The field of modeling active colloids has grown immensely in the past decade (1, 2) and covering the field in its entirety is not possible here. Therefore, in the following we give a personal selection

of current topics, which are in our opinion timely and relevant and likely to become increasingly important in the near future. They rely on the models and methods discussed in the first three sections of this review.

4.1. Crowded and Complex Environments

Although most of the studies on single or collective dynamics of active colloids have been performed in homogeneous fluid environments, recently there has been great interest in understanding active colloidal motion in heterogeneous and complex environments as thoroughly reviewed in Reference 2. Motivations for this are at least twofold. First, active colloids are often used as well-controllable model systems for biological microswimmers, which in their natural habitats often encounter complex environments such as viscoelastic fluids, soil, and various sorts of confinement (2, 91). Second, microscopic active particles may be utilized in the future as smart micromachines operating in complex environments *in vivo* (92). In general, the environment can be modeled as (a) static, realized by fixed walls or obstacles, or (b) dynamic, realized by moving obstacles or polymers dissolved in a Newtonian fluid.

4.1.1. Static environments. Active colloids generically tend to accumulate near large obstacles such as flat walls due to their persistence in swimming (1, 2). In contrast, for relatively small spherical obstacles, active colloids either are scattered off or, for larger obstacle radii, can become trapped and orbit around obstacles due to hydrodynamic colloid–surface interactions (93). In disordered environments consisting of randomly placed obstacles, the long-time diffusion of active colloids strongly depends on the obstacle density and on the specific collision mechanism (94–96). Furthermore, arrays of asymmetrically shaped obstacles rectify the motion or transport of initially randomly oriented active colloids (97), which is a hallmark of active systems operating out of equilibrium.

4.1.2. Complex fluids. Biological microswimmers often have to swim through viscoelastic and shear-thinning fluids (61). Recent investigations have sought to understand how complex structured fluids influence the dynamics of active colloids. On the ABP level, the viscoelastic environment has effectively been modeled using a memory friction kernel in a non-Markovian Langevin equation (98). However, the motion of microswimmers in complex fluids is strongly influenced by the self-generated flow fields (91). In particular, the swimming speed of a squirmer in viscoelastic (99) and shear-thinning (100, 101) fluids depends on not only the first surface-velocity mode B_1 but also higher modes, i.e., crucially on the nature of the self-generated flow field. Furthermore, other studies showed that a nematic environment induces reorientation of a pusher squirmer parallel to the director and of a puller perpendicular to it (102, 103). Finally, microswimmers in the Poiseuille flow of a viscoelastic fluid experience an additional cross-streamline swimming lift that again depends on the neutral or pusher/puller swimmer type (104).

Besides considering continuum models of complex fluids, in recent years efforts have been made to explicitly model polymer solutions and networks with heterogeneous microstructure. For example, the pore size of the polymer network crucially influences the long-time diffusion of ABPs. In particular, sufficiently small pores lead to subdiffusion and trapping (105), similar to ABPs, which become temporally trapped in cages of a static disordered environment (94–96). Using MPCD allows studying the interplay of the polymer microstructure with the self-generated fluid flow of driven or active particles (106–108). A first work on the collective motion of phoretically active microswimmers or nanomotors in polymer networks show enhanced clustering induced by the possibility that the motors are able to attach to the filaments (109).

4.2. Active and Passive Microrheology

Active and passive microrheology is a well-established method for exploring the properties of a complex fluid (see, e.g., Reference 110 for a review). In thermal equilibrium external forcing in the linear-response regime and thermal fluctuations are related by the fluctuation–dissipation theorem, but this is no longer valid for active media. Experiments on passive tracer particles in bacterial baths (111) or in suspensions of the alga *Cblamydomonas reinhardtii* (112) show short-time superdiffusive or ballistic motion followed by strongly enhanced diffusion. These studies also revealed a characteristic property of so-called active baths. The spherical tracer particles are pushed around randomly by the active-bath particles. However, in contrast to a thermal bath the random forces are described by colored noise of the form (111, 113, 114)

$$\langle \xi(t) \rangle = \mathbf{0} \quad \text{and} \quad \langle \xi(t) \otimes \xi(t') \rangle = \mathbf{1} \frac{D^A}{\mu^2 \tau^A} e^{-\frac{|t-t'|}{\tau^A}}. \quad 18.$$

Here, τ^A is of the order of the orientational correlation time, which the active particles need to orient away from the tracer; μ is the mobility of the spherical tracer in the pure solvent; and D^A is its diffusion constant in the active bath. For polar tracers these relations become anisotropic, and a stochastic torque also has to be included.

Recent research concentrated on understanding the properties of an active bath in more detail, where Langevin dynamics simulations of ABPs are crucial. For example, simulations of the passive microrheology of an asymmetric or polar tracer revealed conventional diffusion in the long-time limit (114), whereas theory predicts long-time tails in the active-noise correlations and thereby superdiffusive behavior, which becomes normal diffusion for symmetric tracers (115). Also an extended fluctuation–dissipation theorem for ABPs has been developed (116). Constant-force active microrheology was investigated either by using the low-density description of the active bath based on the Smoluchowski equation, which is equivalent to the Langevin description of ABPs (117), or by employing BD simulations over a wide range of suspension densities (118). Furthermore, experiments did not probe any frequency dependence of the tracer mobility in the active microrheology setting, presumably due to the very low density (113, 119). Most recent simulations, using a broad range for the constant driving force, show a highly nonlinear tracer mobility, where the relevant force scale is the stall force of a half shell of ABPs pushing against the tracer (120). Furthermore, the same work reports a study of oscillatory active microrheology and reveals a frequency dependence of the tracer mobility that can be described by a Lorentzian in the low-frequency domain. Exploring the nonlinear regime and the crossover to linear response as well as the frequency dependence of an active bath provides opportunities for further research.

4.3. Active Colloidal Engines

Active baths described in the previous section exert pressure on a bounding surface or just push against it, which can be harnessed to construct active colloidal engines. The modeling with ABPs as a minimal model of self-propelled particles serves for performing conceptual studies. A recent perspective article by Fodor & Cates reviews the field (121), and they introduce two categories of active engines. First, autonomous engines create motion out of active noise. These are asymmetric objects with grooves, where ABPs or bacteria become trapped so that rotational (122, 123) or translational (114, 124, 125) ratchet motors are realized. Differently shaped polar tracer particles are, e.g., modeled by overlapping spheres or disks, which interact via a hard-core potential with the ABPs (114, 124, 125). Second, active cyclic engines can execute work by performing cyclic changes in a bath of active particles varying, e.g., the stiffness of boundaries and/or the activity of the

particles (meaning the active temperature). An experimental realization of this strategy motivated by the Carnot cycle and the Stirling engine exists (126). The theoretical work of Reference 127 explores extracting the maximum power from an active colloidal heat engine, whereas Reference 128 considers cyclic changes of the particle activity.

Fodor & Cates in Reference 121 also outline future directions of research including developing systematic methods to address the optimization of finite-time cyclic protocols (which they call an outstanding challenge), the investigation of many-body effects, and new realizations of work cycles. Indeed, most recently, active Szilard engines have been introduced that use the information of Maxwell's demon to extract work from an active system. The harnessed work can be much larger than the Landauer value of $k_B T \ln 2$ for thermal Szilard engines when the Péclet number is sufficiently large (129).

4.4. Machine Learning of Active Colloid Navigation

Although self-propelled colloids are able to move actively, i.e., without using external forces, their response to physical environments (phoretic fields, boundaries, external flow, etc.) is purely passive. They translate and rotate according to their surface flow field (Equations 2 and 3) but also due to external driving such as fluid flow and phoretic gradients. This is in contrast to shape-deforming biological microswimmers such as algae or bacteria, which are able to actively adjust their swimming direction by perceiving information from their environment through different receptors and using an internal decision-making machinery.

Nevertheless, even for a single active colloid, which cannot make decisions on its own, an external information processing unit may be coupled to the colloid. It monitors the state of the colloid, decides on its reorientation, and then takes the required action. In an experimental realization the state of a self-thermophoretic active colloid was observed by a microscope, which was coupled to a laser to locally heat the colloid and thereby reorient it (130). Reinforcement learning (RL) based on the Q-matrix approach was used to obtain the optimal action for each state in order to perform an optimization task. Thus, the goal is to develop more advanced, smart micromachines, which make independent decisions based on internal sensing and thereby perform tasks without external guidance (92).

Theoretical modeling of active colloid navigation in different environments has also successfully used RL in connection with the ABP model. It is assumed that the active colloid has an internal machinery to sense the environment in order to decide and perform a change in direction or intrinsic speed. Constructing such a machinery based on physical mechanisms constitutes a major challenge. To perform an optimization task with RL, a simple Q-learning procedure (131), deep neural networks (132), or networks evolved by genetic algorithms (133) are used. Based on RL, ABPs have been trained to optimally navigate in external fluid flow (131, 134–136), in external potentials (137), in crowded environments (132), to control collective transport (138), and to optimally cloak a prey against a predator using cloaking agents and hydrodynamic far-field interactions (139).

Most recent works go beyond the ABP model and provide an explicit reorientation mechanism of microswimmers in a hydrodynamic environment. They either use bioinspired shape-deforming microswimmers, which have been trained to adjust their swimming strokes in response to environmental conditions (133, 140), or rely on the squirmer that uses different state-dependent surface velocity fields to modulate speed and orientation (141).

4.5. Effects of Inertia

So far, we have considered active particles without inertia, meaning in the overdamped case. However, recently also inertial effects of active particles have come into focus as reviewed in

Reference 142, in particular, in connection with dry active matter and active walkers (143). Macroscopic active particles with inertia have been studied under confinement for two cases, camphor surfers and hexbug crawlers, with the surprising result that in contrast to ABPs the surfers are not preferentially stuck at the boundary but on average a distance away from it due to their epicycle dynamics (144). Also, the influence of inertia on phase separation (145) and, in particular, MIPS (142) has been investigated, showing that inertia hinders clustering.

The equations for adding inertia to active particles were first formulated in Reference 146:

$$\begin{aligned}\dot{\mathbf{r}} &= \mathbf{v}, & \dot{\mathbf{v}} &= -\frac{\gamma}{m}(\mathbf{v} - v_0\mathbf{e}) + \boldsymbol{\omega} \times v_0\mathbf{e} + \frac{1}{m}\mathbf{F} + \boldsymbol{\zeta}, \\ \dot{\mathbf{e}} &= \boldsymbol{\omega} \times \mathbf{e}, & \dot{\boldsymbol{\omega}} &= -\frac{\gamma_r}{I}\boldsymbol{\omega} + \boldsymbol{\eta}.\end{aligned}\tag{19}$$

When the translational and rotational accelerations $\boldsymbol{\zeta}$ and $\boldsymbol{\eta}$ are of thermal origin, their second moments fulfill the fluctuation–dissipation theorem: $\langle \boldsymbol{\zeta}(t) \otimes \boldsymbol{\zeta}(t') \rangle = (2\gamma k_B T/m^2)\delta(t - t')\mathbf{I}$ and $\langle \boldsymbol{\eta}(t) \otimes \boldsymbol{\eta}(t') \rangle = (2\gamma_r k_B T/I^2)\delta(t - t')\mathbf{I}$. The pseudoacceleration term $\boldsymbol{\omega} \times v_0\mathbf{e}$ is reminiscent of a Coriolis force but also present in an inertial frame. Using the first equation in the second line, one can rewrite it together with the inertial term as $d(\mathbf{v} - v_0\mathbf{e})/dt$. Thus, the forces only generate acceleration relative to self-propulsion, which makes sense. The pseudoacceleration term has been added in Reference 147 to describe dry active particles in the noninertial frame of a rotating disk, where $\boldsymbol{\omega}$ is replaced by the angular velocity of the disk. Otherwise, the consequences of this term have not been investigated so far. It should become relevant in so-called circle swimmers with an intrinsic active rotation (38, 148) or when an external torque and/or rotational noise acts on the particle.

Other studies have concentrated on the effect of fluid inertia while swimmer inertia can still be ignored. In particular, the dependence of the swimming velocity of a squirmer expanded into the Reynolds number was calculated in References 149 and 150. The field of inertial microfluidics uses so-called inertial lift forces for cell sorting and flow cytometry techniques. They are due to fluid inertia, cause cross-stream migration in a Poiseuille flow, and focus particles halfway between channel center and wall. Here again, particle inertia can be ignored. A recent article has generalized these lift forces to microswimmers, also introducing an inertial swimming lift (151). Depending on the swimmer type, a rich spectrum of complex dynamics including bistable states, where tumbling coexists with stable centerline swimming or swinging, has been identified.

5. CONCLUSIONS

We have reviewed methods to model the motion of interacting active colloids by discussing different levels of approximations. They range from the generic ABP model, where effective hydrodynamic and phoretic interactions can be included mainly in the far-field approximation, to explicit modeling approaches, which fulfill the exact boundary conditions of the involved hydrodynamic and phoretic fields even when active colloids come close to each other so that near-field interactions are needed. These modeling approaches on the particle level are versatile and we illustrated their use with selected current topics in the field of active matter and microswimmers that promise to advance the field.

SUMMARY POINTS

1. Active colloids swim by creating self-generated fluid flows induced by local gradients of phoretic fields close to the colloids.

2. The generic model of ABPs can include hydrodynamic and phoretic interactions in the far-field approximation.
3. Explicit modeling of hydrodynamic and phoretic fields is necessary for dense systems and to access the full hydrodynamic-chemical coupling.
4. Selected current topics using the modeling of active colloids include the following: (a) motion in crowded and complex environments, (b) microrheology in active baths, (c) active colloidal engines, (d) adaptive response of active colloids using machine learning techniques, and (e) effects of colloid and fluid inertia.

DISCLOSURE STATEMENT

The authors are not aware of any affiliations, memberships, funding, or financial holdings that might be perceived as affecting the objectivity of this review.

ACKNOWLEDGMENTS

We apologize to the many colleagues whose work could not be cited appropriately owing to space constraints. We thank all our colleagues for inspiring collaborations and discussions in the last years. H.S. thanks the Deutsche Forschungsgemeinschaft for funding through the priority program SPP 1726 (grant number STA352/11).

LITERATURE CITED

1. Zöttl A, Stark H. 2016. *J. Phys. Condens. Matter* 28:253001
2. Bechinger C, Di Leonardo R, Löwen H, Reichhardt C, Volpe G, Volpe G. 2016. *Rev. Mod. Phys.* 88:045006
3. Mallory SA, Valeriani C, Cacciuto A. 2018. *Annu. Rev. Phys. Chem.* 69:59–79
4. Lauga E, Powers TR. 2009. *Rep. Prog. Phys.* 72:096601
5. Narayan V, Ramaswamy S, Menon N. 2007. *Science* 317:105–8
6. Anderson JL. 1989. *Annu. Rev. Fluid Mech.* 21:61–99
7. Moran JL, Posner JD. 2017. *Annu. Rev. Fluid Mech.* 49:511–40
8. Illien P, Golestanian R, Sen A. 2017. *Chem. Soc. Rev.* 46:5508–18
9. Soto R, Golestanian R. 2014. *Phys. Rev. Lett.* 112:068301
10. Michelin S, Lauga E, Bartolo D. 2013. *Phys. Fluids* 25:061701
11. Golestanian R, Liverpool TB, Ajdari A. 2007. *New J. Phys.* 9:126
12. Jiang HR, Yoshinaga N, Sano M. 2010. *Phys. Rev. Lett.* 105:268302
13. Bickel T, Majee A, Würger A. 2013. *Phys. Rev. E* 88:012301
14. Kroy K, Chakraborty D, Cichos F. 2016. *Eur. Phys. J. Spec. Top.* 225:2207–25
15. Lozano C, ten Hagen B, Löwen H, Bechinger C. 2016. *Nat. Commun.* 7:12828
16. Stone H, Samuel A. 1996. *Phys. Rev. Lett.* 77:4102–4
17. Spagnolie SE, Lauga E. 2012. *J. Fluid. Mech.* 700:105–47
18. Campbell AI, Ebbens SJ, Illien P, Golestanian R. 2019. *Nat. Commun.* 10:3952
19. Ishikawa T, Simmonds MP, Pedley TJ. 2006. *J. Fluid Mech.* 568:119–60
20. Yoshinaga N, Liverpool TB. 2017. *Phys. Rev. E* 96:020603(R)
21. Golestanian R. 2012. *Phys. Rev. Lett.* 108:038303
22. Pohl O, Stark H. 2015. *Eur. Phys. J. E* 38(8):93
23. Marchetti MC, Joanny JF, Ramaswamy S, Liverpool TB, Prost J, et al. 2013. *Rev. Mod. Phys.* 85:1143–89
24. Sharifi-Mood N, Mozaffari A, Córdova-Figueroa UM. 2016. *J. Fluid Mech.* 798:910–54

25. Varma A, Michelin S. 2019. *Phys. Rev. Fluids* 4:124204. <https://doi.org/10.1103/PhysRevFluids.4.124204>
26. Redner GS, Baskaran A, Hagan MF. 2013. *Phys. Rev. E* 88:012305
27. Buttinoni I, Bialké J, Kümmel F, Löwen H, Bechinger C, Speck T. 2013. *Phys. Rev. Lett.* 110:238301
28. Digregorio P, Levis D, Suma A, Cugliandolo LF, Gonnella G, Pagonabarraga I. 2018. *Phys. Rev. Lett.* 121:098003
29. Cates ME, Tailleur J. 2015. *Annu. Rev. Condens. Matter Phys.* 6:219–44
30. Fily Y, Marchetti MC. 2012. *Phys. Rev. Lett.* 108:235702
31. Blaschke J, Maurer M, Menon K, Zöttl A, Stark H. 2016. *Soft Matter* 12:9821–31
32. Stenhammar J, Marenduzzo D, Allen RJ, Cates ME. 2014. *Soft Matter* 10:1489–99
33. Wysocki A, Winkler RG, Gompper G. 2014. *Europhys. Lett.* 105:48004
34. Suma A, Gonnella G, Marenduzzo D, Orlandini E. 2014. *Europhys. Lett.* 108:56004
35. Baskaran A, Marchetti MC. 2008. *Phys. Rev. Lett.* 101:268101
36. Wensink HH, Löwen H. 2012. *J. Phys. Condens. Matter* 24:464130
37. Bär M, Großmann R, Heidenreich S, Peruani F. 2020. *Annu. Rev. Condens. Matter Phys.* 11:441–66
38. van Teeffelen S, Löwen H. 2008. *Phys. Rev. E* 78:020101(R)
39. Kümmel F, ten Hagen B, Wittkowski R, Buttinoni I, Eichhorn R, et al. 2013. *Phys. Rev. Lett.* 110:198302
40. Nguyen NHP, Klotsa D, Engel M, Glotzer SC. 2014. *Phys. Rev. Lett.* 112:075701
41. Yeo K, Lushi E, Vlahovska PM. 2015. *Phys. Rev. Lett.* 114:188301
42. Goto Y, Tanaka H. 2015. *Nat. Commun.* 6:5994
43. Theurkauff I, Cottin-Bizonne C, Palacci J, Ybert C, Bocquet L. 2012. *Phys. Rev. Lett.* 108:268303
44. Palacci J, Sacanna S, Vatchinsky A, Chaikin PM, Pine DJ. 2013. *J. Am. Chem. Soc.* 135:15978–81
45. Mognetti BM, Šarić A, Angioletti-Uberti S, Cacciuto A, Valeriani C, Frenkel D. 2013. *Phys. Rev. Lett.* 111:245702
46. Alarcón F, Valeriani C, Pagonabarraga I. 2017. *Soft Matter* 13:814–26
47. Pohl O, Stark H. 2014. *Phys. Rev. Lett.* 112:238303
48. Saha S, Golestanian R, Ramaswamy S. 2014. *Phys. Rev. E* 89:62316
49. Stürmer J, Seyrich M, Stark H. 2019. *J. Chem. Phys.* 150:214901
50. Hennes M, Wolff K, Stark H. 2014. *Phys. Rev. Lett.* 112:238104
51. Ishikawa T. 2009. *J. R. Soc. Interface* 6:815–34
52. Zöttl A, Stark H. 2014. *Phys. Rev. Lett.* 112:118101
53. Kyoya K, Matsunaga D, Imai Y, Omori T, Ishikawa T. 2015. *Phys. Rev. E* 92:63027
54. Lighthill JM. 1952. *Commun. Pure Appl. Math.* 5:109–18
55. Blake JR. 1971. *Math. Proc. Camb. Philos. Soc.* 70:303
56. Pak OS, Lauga E. 2014. *J. Eng. Math.* 88:1–28
57. Schmitt M, Stark H. 2016. *Phys. Fluids* 28:012106
58. Evans AA, Ishikawa T, Yamaguchi T, Lauga E. 2011. *Phys. Fluids* 23:111702
59. Delmotte B, Keaveny EE, Plouraboué F, Climent E. 2015. *J. Comput. Phys.* 302:524–47
60. Matas-Navarro R, Golestanian R, Liverpool TB, Fielding SM. 2014. *Phys. Rev. E* 90:032304
61. Li G, Ostace A, Ardekani AM. 2016. *Phys. Rev. E* 94:053104
62. Zöttl A. 2020. *Chin. Phys. B* 29:074701
63. Llopis I, Pagonabarraga I. 2010. *J. Non-Newtonian Fluid Mech.* 165:946–52
64. Kuron M, Stärk P, Burkard C, De Graaf J, Holm C. 2019. *J. Chem. Phys.* 150:144110
65. Downton MT, Stark H. 2009. *J. Phys. Condens. Matter* 21:204101
66. Götze IO, Gompper G. 2010. *Phys. Rev. E* 82:041921
67. Zöttl A, Stark H. 2012. *Phys. Rev. Lett.* 108:218104
68. Zantop AW, Stark H. 2021. *J. Chem. Phys.* 154:024105
69. Theers M, Westphal E, Qi K, Winkler RG, Gompper G. 2018. *Soft Matter* 14:8590–603
70. Kuhr JT, Rühle F, Stark H. 2019. *Soft Matter* 15:5685–94
71. Qi K, Westphal E, Gompper G, Winkler RG. 2022. *Commun. Phys.* 5:49
72. Kuhr JT, Blaschke J, Rühle F, Stark H. 2017. *Soft Matter* 13:7548–55
73. Rühle F, Stark H. 2020. *Eur. Phys. J. E* 43:26

74. Zantop AW, Stark H. 2021. *J. Chem. Phys.* 155:134904
75. Zantop A, Stark H. 2022. *Soft Matter* 18:6179–91
76. Alarcón F, Pagonabarraga I. 2013. *J. Mol. Liq.* 185:56–61
77. Popescu MN, Uspal WE, Eskandari Z, Tasinkevych M, Dietrich S. 2018. *Eur. Phys. J. E* 41:145
78. Varma A, Montenegro-Johnson TD, Michelin S. 2018. *Soft Matter* 14:7155–73
79. Schmitt M, Stark H. 2013. *Europhys. Lett.* 101:44008
80. Uspal WE, Popescu MN, Dietrich S, Tasinkevych M. 2015. *Soft Matter* 11:434–38
81. Mozaffari A, Sharifi-Mood N, Koplik J, Maldarelli C. 2016. *Phys. Fluids* 28:053107
82. Popescu MN, Tasinkevych M, Dietrich S. 2011. *Europhys. Lett.* 95:28004
83. Reigh SY, Kapral R. 2015. *Soft Matter* 11:3149–58
84. Liebchen B, Löwen H. 2019. *J. Chem. Phys.* 150:061102
85. Kanso E, Michelin S. 2019. *J. Chem. Phys.* 150:044902
86. Thakur S, Kapral R. 2012. *Phys. Rev. E* 85:026121
87. Huang MJ, Schofield J, Gaspard P, Kapral R. 2019. *J. Chem. Phys.* 150(12):124110
88. Wagner M, Roca-Bonet S, Ripoll M. 2021. *Eur. Phys. J. E* 44(3):43
89. Scagliarini A, Pagonabarraga I. 2020. *Soft Matter* 16:8893–903
90. Rojas-Pérez F, Delmotte B, Michelin S. 2021. *J. Fluid Mech.* 919:A22
91. Li G, Lauga E, Ardekani AM. 2021. *J. Non-Newtonian Fluid Mech.* 297:104655
92. Huang TY, Gu H, Nelson BJ. 2022. *Annu. Rev. Control Robot. Auton. Syst.* 5:279–310
93. Spagnolie SE, Moreno-Flores GR, Bartolo D, Lauga E. 2015. *Soft Matter* 11:3396–411
94. Chepizhko O, Peruani F. 2013. *Phys. Rev. Lett.* 111:160604
95. Zeitz M, Wolff K, Stark H. 2017. *Eur. Phys. J. E* 40:23
96. Morin A, Lopes Cardozo D, Chikkadi V, Bartolo D. 2017. *Phys. Rev. E* 96:042611
97. Reichhardt CJ, Reichhardt C. 2017. *Annu. Rev. Condens. Matter Phys.* 8:51–75
98. Narinder N, Bechinger C, Gomez-Solano JR. 2018. *Phys. Rev. Lett.* 121:078003
99. Zhu L, Lauga E, Brandt L. 2012. *Phys. Fluids* 24:051902
100. Montenegro-Johnson TD, Smith DJ, Loghin D. 2013. *Phys. Fluids* 25:081903
101. Datt C, Zhu L, Elfring GJ, Pak OS. 2015. *J. Fluid Mech.* 784:R1
102. Lintuvuori JS, Würger A, Stratford K. 2017. *Phys. Rev. Lett.* 119:068001
103. Mandal S, Mazza MG. 2021. *Eur. Phys. J. E* 44:64
104. Choudhary A, Stark H. 2022. *Soft Matter* 18:48–52
105. Du Y, Jiang H, Hou Z. 2019. *Soft Matter* 15:2020–31
106. Zöttl A, Yeomans JM. 2019. *J. Phys. Condens. Matter* 31:234001
107. Zöttl A, Yeomans JM. 2019. *Nat. Phys.* 15:554–58
108. Qi K, Westphal E, Gompper G, Winkler RG. 2020. *Phys. Rev. Lett.* 124:068001
109. Qiao L, Huang MJ, Kapral R. 2020. *Phys. Rev. Res.* 2:033245
110. Zia RN. 2018. *Annu. Rev. Fluid Mech.* 50:371–405
111. Wu XL, Libchaber A. 2000. *Phys. Rev. Lett.* 84:3017–20
112. Leptos KC, Guasto JS, Gollub JP, Pesci AI, Goldstein RE. 2009. *Phys. Rev. Lett.* 103:198103
113. Maggi C, Paoluzzi M, Angelani L, Di Leonardo R. 2017. *Sci. Rep.* 7:17588
114. Knežević M, Stark H. 2020. *New J. Phys.* 22:113025
115. Granek O, Kafri Y, Tailleur J. 2022. *Phys. Rev. Lett.* 129:038001
116. Cengio SD, Levis D, Pagonabarraga I. 2019. *Phys. Rev. Lett.* 123:238003
117. Burkholder EW, Brady JF. 2020. *Soft Matter* 16:1034–46
118. Reichhardt C, Olson Reichhardt CJ. 2015. *Phys. Rev. E* 91:032313
119. Chen DTN, Lau AWC, Hough LA, Islam MF, Goulian M, et al. 2007. *Phys. Rev. Lett.* 99:148302
120. Knežević M, Avilés Podgurski LE, Stark H. 2021. *Sci. Rep.* 11:22706
121. Fodor T, Cates ME. 2021. *Europhys. Lett.* 134:10003
122. Di Leonardo R, Angelani L, Dell’Arciprete D, Ruocco G, Schippa S, et al. 2010. *PNAS* 107:9541–45
123. Sokolov A, Apodaca MM, Grzybowski BA, Aranson IS. 2010. *PNAS* 107:969–74
124. Angelani L, Di Leonardo R. 2010. *New J. Phys.* 12:113017
125. Kaiser A, Peshkov A, Sokolov A, ten Hagen B, Löwen H, Aranson IS. 2014. *Phys. Rev. Lett.* 112:158101

126. Krishnamurthy S, Ghosh S, Chatterji D, Ganapathyand R, Sood AK. 2016. *Nat. Phys.* 12:1134–39
127. Martin D, Nardini C, Cates M, Fodor É. 2018. *Europhys. Lett.* 121:60005
128. Malgaretti P, Nowakowski P, Stark H. 2021. *Europhys. Lett.* 134:20002
129. Malgaretti P, Stark H. 2022. *Phys. Rev. Lett.* 129:228005
130. Muiños-Landin S, Fischer A, Holubec V, Cichos F. 2021. *Sci. Robot.* 6:eabd9285
131. Colabrese S, Gustavsson K, Celani A, Biferale L. 2017. *Phys. Rev. Lett.* 118:158004
132. Yang Y, Bevan MA, Li B. 2020. *Adv. Intel. Syst.* 2:1900106
133. Hartl B, Hübl M, Kahl G, Zöttl A. 2021. *PNAS* 118:e2019683118
134. Alageshan JK, Verma AK, Bec J, Pandit R. 2020. *Phys. Rev. E* 101:043110
135. Gunnarson P, Mandralis I, Novati G, Koumoutsakos P, Dabiri JO. 2021. *Nat. Commun.* 12:7143
136. Nasiri M, Liebchen B. 2022. *New J. Phys.* 24:073042
137. Schneider E, Stark H. 2019. *Europhys. Lett.* 127:64003
138. Falk MJ, Alizadehyazdi V, Jaeger H, Murugan A. 2021. *Phys. Rev. Res.* 3:033291
139. Mirzakanloo M, Esmacilzadeh S, Alam MR. 2020. *J. Fluid Mech.* 903:A34
140. Tsang ACH, Tong PW, Nallan S, Pak OS. 2020. *Phys. Rev. Fluids* 5:074101
141. Zhu G, Fang WZ, Zhu L. 2022. *J. Fluid. Mech.* 944:A3
142. Löwen H. 2020. *J. Chem. Phys.* 152:040901
143. Scholz C, Jahanshahi S, Ldov A, Löwen H. 2018. *Nat. Commun.* 9:5156
144. Leoni M, Paoluzzi M, Eldeen S, Estrada A, Nguyen L, et al. 2020. *Phys. Rev. Res.* 2:043299
145. Dai C, Bruss IR, Glotzer SC. 2020. *Soft Matter* 16:2847–53
146. Enculescu M, Stark H. 2011. *Phys. Rev. Lett.* 107:058301
147. Löwen H. 2019. *Phys. Rev. E* 99:062608
148. Chepizhko O, Franosch T. 2019. *Soft Matter* 15:452–61
149. Wang S, Ardekani A. 2012. *Phys. Fluids* 24:101902
150. Khair AS, Chisholm NG. 2014. *Phys. Fluids* 26:011902
151. Choudhary A, Paul S, Rühle F, Stark H. 2022. *Commun. Phys.* 5:14